

Active flux for triangular meshes for compressible flows problems

Rémi Abgrall, Jianfang Lin and Yongle Liu
 Institute of Mathematics, University of Zürich, Switzerland
 {remi.abgrall,jianfang.lin,yongle.liu}@math.uzh.ch

Abstract

In this article, we show how to construct a numerical method for solving hyperbolic problems, whether linear or non-linear, using a continuous representation of the variables and their mean value in each triangular element. This type of approach has already been introduced by Roe, and others, in the multi-dimensional framework under the name of Active Flux, see [11, 12, 10, 16, 7]. Here, the presentation is more general and follows [4, 6]. Various examples show the good behavior of the method in both linear and non-linear cases, including non-convex problems. The expected order of precision is obtained in both the linear and non-linear cases. This work represents a step towards the development of methods in the spirit of virtual finite elements for linear or non-linear hyperbolic problems, including the case where the solution is not regular.

1 Introduction

A new numerical method for solving hyperbolic problems was first introduced in [11, 12, 10]. This new method uses the degrees of freedom (DoFs) of the quadratic polynomials, which are all on the boundary of the elements, and another degree of freedom that used is the cell average of the solution. This leads to a potentially third-order method, with a globally continuous approximation. The time integration relies on a back-tracing of characteristics. This has been extended to square elements, in a finite difference fashion, in [16, 7]. In [4], a different, though very close, point of view is followed. The time stepping relies on a standard Runge-Kutta time stepping, and several versions of the same problem can be used without preventing local conservation. More precisely, a conservative version of the studied problem is used to update the average value and the local conservation property is guaranteed. In addition, we have more flexibility for the DoFs on the boundary of the elements. Namely, we can use several versions of the same problem, such as the primitive formulation, to update these DoFs. This is benefit from the fact that the point values are free of the local conservation and we do not need to be restricted by the conservation formulation. These routes have been followed in [6] which gives several versions of higher order approximation, in one dimension.

The purpose of this paper is to extend the work of [4] to several dimensions, using simplex elements. We first describe the approximation space, then propose a discretization method, with some justifications, and then show numerical examples. We also show how to handle discontinuous solutions.

The hyperbolic problems we consider are written in a conservative form as:

$$\frac{\partial \mathbf{u}}{\partial t} + \operatorname{div} \mathbf{f}(\mathbf{u}) = 0, \quad \mathbf{x} \in \Omega \subset \mathbb{R}^d, \quad (1)$$

with $d = 2$, complemented by initial conditions

$$\mathbf{u}(\mathbf{x}, 0) = \mathbf{u}_0(\mathbf{x}), \quad \mathbf{x} \in \Omega,$$

and boundary conditions that will be described case-by-case. The solution $\mathbf{u} \in \mathbb{R}^m$ must stay in an open subspace $\mathcal{D} \subset \mathbb{R}^d$ so that the flux \mathbf{f} is defined. This is the invariant domain.

Two sets of problems are considered:

- the case of scalar conservation law with \mathbf{f} linear taking the form of $\mathbf{f}(\mathbf{u}, \mathbf{x}) = \mathbf{a}(\mathbf{x})\mathbf{u}$ or non-linear. In that case, \mathbf{u} is a function with values in \mathbb{R} and $\mathcal{D} = \mathbb{R}$ but the solution must stay in $[\min_{\mathbf{x} \in \mathbb{R}} \mathbf{u}_0(\mathbf{x}), \max_{\mathbf{x} \in \mathbb{R}} \mathbf{u}_0(\mathbf{x})]$, due to Kruzhkov's theory: in these particular examples, we set $\mathcal{D} = [\min_{\mathbf{x} \in \mathbb{R}} \mathbf{u}_0(\mathbf{x}), \max_{\mathbf{x} \in \mathbb{R}} \mathbf{u}_0(\mathbf{x})]$.
- the case of the Euler equations, where $\mathbf{u} = (\rho, \rho\mathbf{v}, E)$, ρ is the density, \mathbf{v} is the velocity, and E is the total energy, i.e., the sum of the internal energy e and the kinetic energy $\frac{1}{2}\rho\mathbf{v}^2$. The flux is

$$\mathbf{f}(\mathbf{u}) = \begin{pmatrix} \rho\mathbf{v} \\ \rho\mathbf{v} \otimes \mathbf{v} + p\text{Id}_d \\ (E + p)\mathbf{v} \end{pmatrix}$$

with Id_d being a $d \times d$ identity matrix. We have introduced the pressure that is related to the internal energy and the density by an equation of state. Here we make the choice of a perfect gas,

$$p = (\gamma - 1)e$$

with γ denoting the specific heat ratio. In all of the numerical examples tested in §4.2, we have taken $\gamma = 1.4$. In this example, $\mathcal{D} = \{\mathbf{u} \in \mathbb{R}^4, \rho > 0, e > 0\}$.

We note that for smooth solutions, (1) can be re-written in a non-conservative form,

$$\frac{\partial \mathbf{u}}{\partial t} + \mathbf{J} \cdot \nabla \mathbf{u} = 0,$$

where

$$\mathbf{J} \cdot \nabla \mathbf{u} = A \frac{\partial \mathbf{u}}{\partial x} + B \frac{\partial \mathbf{u}}{\partial y},$$

with A and B being the Jacobians of the flux in the x - and y - direction, respectively. The system is hyperbolic, i.e., for any vector $\mathbf{n} = (n_x, n_y)$, the matrix

$$\mathbf{J} \cdot \mathbf{n} = An_x + Bn_y$$

is diagonalisable in \mathbb{R} .

2 Approximation space

For now, we consider a triangle E and the corresponding quadratic polynomial approximation. The degrees of freedom are the vertices $\sigma_i, i = 1, \dots, 3$, the midpoints $\sigma_i, i = 4, \dots, 6$, and the average, see Figure 1. The first question whether we can find a polynomial space V that contains at least the quadratic polynomials, and something more, in order to accommodate the average value as an independent variable, that is if we can find 7 polynomials (φ_i) such that

$$\varphi_i(\sigma_j) = \delta_i^j \text{ for } 1 \leq i, j \leq 6, \quad \int_E \varphi_i(\mathbf{x}) \, d\mathbf{x} = 0 \text{ for } i = 1, \dots, 6, \quad (2)$$

and

$$\varphi_7(\sigma_j) = 0, \quad \int_E \varphi_7(\mathbf{x}) \, d\mathbf{x} = |E|. \quad (3)$$

An obvious choice is $\varphi_7 = 60\lambda_1\lambda_2\lambda_3$ with $(\lambda_1, \lambda_2, \lambda_3)$ being the barycentric coordinates and $\varphi_i =$ the Lagrange basis function $+\beta_i\varphi_7$ with β_i well chosen.

More precisely, the quadratic Lagrange polynomials are $\varphi_i^L(\mathbf{x}) = \lambda_i(2\lambda_i - 1)$, $i = 1, 2, 3$ and $\varphi_4^L = 4\lambda_1\lambda_2$, $\varphi_5^L = 4\lambda_2\lambda_3$ and $\varphi_6^L = 4\lambda_1\lambda_3$. Since

$$\int_E \varphi_i^L \, d\mathbf{x} = 0,$$

for $i = 1, 2, 3$, we set $\varphi_i = \varphi_i^L$. Similarly, we see that we can set

$$\varphi_i = \varphi_i^L - \frac{1}{3}\varphi_7,$$

for $i = 4, 5, 6$. It is trivial to verify that the above-mentioned polynomials φ_i satisfy the conditions (2) and (3). Therefore, these polynomials serve as the quadratic basis functions of the polynomial space V .

The same idea can be extended to tetrahedrons and higher than quadratic degree. For example, we can get a cubic approximation by taking 9 Lagrange points with barycentric coordinates $(\frac{i}{3}, \frac{j}{3}, \frac{k}{3})$ with $i+j+k = 3$ and at least one among the $\{i, j, k\}$ being set to 0 so that we are on the boundary of the triangle E , and the average value. Hence the polynomials are:

$$\varphi_{10} = 60\lambda_1\lambda_2\lambda_3,$$

and

$$\varphi_i = \frac{1}{2}\lambda_i(3\lambda_i - 1)(3\lambda_i - 2) - 2\lambda_1\lambda_2\lambda_3, \quad \text{for } i = 1, 2, 3,$$

then

$$\varphi_4 = \frac{9}{2}\lambda_1\lambda_2(3\lambda_1 - 1) - \frac{9}{2}\lambda_1\lambda_2\lambda_3,$$

$$\varphi_5 = \frac{9}{2}\lambda_1\lambda_2(3\lambda_2 - 1) - \frac{9}{2}\lambda_1\lambda_2\lambda_3,$$

and the others $\{\varphi_6, \varphi_7, \varphi_8, \varphi_9\}$ are obtained by symmetry.

Our notations will be \mathbf{u}_σ for the point values and $\bar{\mathbf{u}}_E$ for the cell average. Finally, the solution \mathbf{u} can be approximated in each element by

$$\mathbf{u} \approx \sum_{i=1}^6 \mathbf{u}_{\sigma_i} \varphi_i + \bar{\mathbf{u}}_E \varphi_7, \quad (4)$$

for the third-order approximation and

$$\mathbf{u} \approx \sum_{i=1}^9 \mathbf{u}_{\sigma_i} \varphi_i + \bar{\mathbf{u}}_E \varphi_{10}, \quad (5)$$

for the fourth-order approximation.

3 Numerical schemes

In this section, we describe how to evolve in time the degrees of freedom. We use the method of line, with a SSP Runge-Kutta (third-order) in time. In the following, we describe the spatial discretization. We first describe a high-order version, and then a first-order one.

3.1 High order schemes

The update of the average values is done by using the conservative formulation, i.e.,

$$\frac{\partial \mathbf{u}}{\partial t} + \text{div} \mathbf{f}(\mathbf{u}) = 0, \quad (6)$$

both the conservative and a non-conservative version of the same system

$$\frac{\partial \mathbf{u}}{\partial t} + \mathbf{J} \cdot \nabla \mathbf{u} = 0. \quad (7)$$

On a triangle E , \mathbf{u} is represented by point values at the Lagrange DoFs and its average on the element. The function \mathbf{u} is a quadratic or cubic polynomial on each element, so that the update is done via:

$$|E| \frac{d\bar{\mathbf{u}}_E}{dt} + \oint_{\partial E} \mathbf{f}(\mathbf{u}) \cdot \mathbf{n} \, d\ell = 0, \quad (8)$$

where the integral is obtained by using quadrature formula on each edge. In our simulations, we use a Gaussian quadrature formula with 3 Gaussian points on each edge, so that there is no loss of accuracy.

The update of the boundary values is more involved and we describe several solutions. Inspired by Residual Distribution schemes, and in particular the LDA (Low Diffusion advection A) scheme [9]¹, one can define, for each of the polynomial DoFs $\sigma \in \{\sigma_1, \sigma_2, \dots\}$ over the element E ,

$$\Phi_\sigma^E(\mathbf{u}) = (K_\sigma^E)^+ N_\sigma(\mathbf{J}(\mathbf{u}_\sigma) \cdot \nabla \mathbf{u}), \quad N_\sigma^{-1} = \sum_{\sigma \in E} (K_\sigma^E)^+,$$

where, since the problem is hyperbolic and whatever the vector \mathbf{n}_σ^E , one can take the positive and negative parts of K_σ^E

$$K_\sigma^E = (K_\sigma^E)^- + (K_\sigma^E)^+ = R\Lambda R^{-1} = R\Lambda^- R^{-1} + R\Lambda^+ R^{-1},$$

with

$$\begin{aligned} \Lambda^- &= \text{diag}(\min(\lambda_1, 0), \dots, \min(\lambda_m, 0)), \\ \Lambda^+ &= \text{diag}(\max(\lambda_1, 0), \dots, \max(\lambda_m, 0)), \\ K_\sigma^E &= \mathbf{J}(\mathbf{u}_\sigma) \cdot \mathbf{n}_\sigma^E. \end{aligned}$$

This normal vector, see Figure 1, is defined as follows:

- for the quadratic approximation where we have used the DoFs of quadratic polynomials on the edges of the element, if σ is a vertex, \mathbf{n}_σ is the inward normal to the opposite edge of σ , if σ is a mid point, this is the outward normal to the edge where σ is sitting.
- for the cubic approximation where we have used the DoFs of cubic polynomials on the edges of the element, we apply the same procedure, described in the above case of quadratic approximation, to the vertices and the other DoFs on edges.

These two procedures can be reduced to the following. We notice that a degree of freedom belongs to two edges, the one sitting on its left and the one sitting on its right. These two edges can be identical. We then define the normal by adding the scaled normals of the outward normals to these edges.

Once this is done, we update \mathbf{u} by the following

$$\frac{d\mathbf{u}_\sigma}{dt} + \sum_{E, \sigma \in E} \Phi_\sigma^E = 0.$$

The idea behind is to have some up-winding mechanism, however, the consistency is not clear: if we have a linear \mathbf{u} , i.e., with $\nabla \mathbf{u}$ constant, we would like to recover

$$\sum_{E, \sigma \in E} \Phi_\sigma^E = \mathbf{J}(\mathbf{u}_\sigma) \cdot \nabla \mathbf{u}.$$

A priori, there is no reason for this. Hence a better idea is:

¹The LDA scheme (LDA standing for Low Diffusion advection A scheme, there were a B and C version) is a scheme specialized to steady advection problems on triangular meshes for scalar problems. Point value residual are defined to update the solution in a way similar as we do here. It is locally conservative, high-order and upwind but does not prevent spurious oscillations at discontinuities. It is the second order in its original version. The accuracy is obtained by defining the residual at this point as the product of the upwind parameter with $J \cdot \nabla u$. The upwind property is obtained by looking at the sign of the scalar product of local velocity (hence J for a scalar problem) against the normal opposite to the vertex for which we evaluate the residual. Finally local conservation is guaranteed by multiplying the upwind parameter by a scaling factor, the so-called N parameter, so that the sum or the fluctuations over the element is equal to $\int_E J \cdot \nabla u \, dx$. The J Jacobians are evaluated so that this integral is equal to the integral over the boundary of the normal flux, by some generalization of the Roe average. An extension for systems was defined later in van der Weide's PhD thesis[22], see also [23].

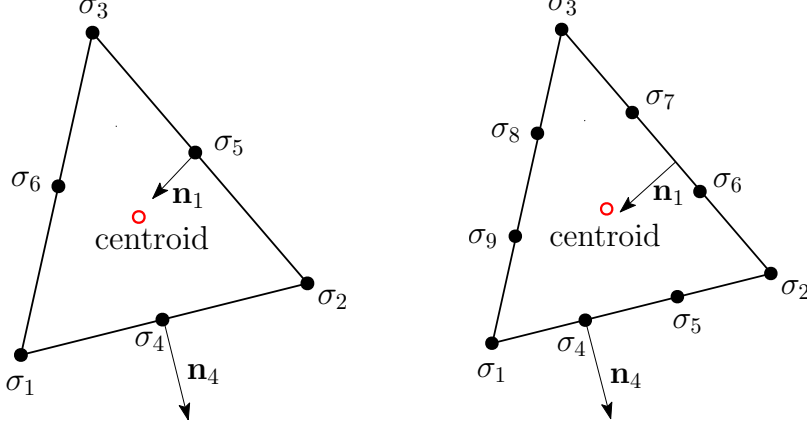


Figure 1: Normals for (9). Left: quadratic; Right: cubic.

$$\frac{d\mathbf{u}_\sigma}{dt} + \sum_{E, \sigma \in E} \Phi_\sigma^E(\mathbf{u}) = 0, \quad (9a)$$

with

$$\Phi_\sigma^E(\mathbf{u}) = N_\sigma (K_\sigma^E)^+ \mathbf{J}(\mathbf{u}_\sigma) \cdot \nabla \mathbf{u}(\sigma), \quad (9b)$$

$$K_\sigma^E = \mathbf{J}(\mathbf{u}_\sigma) \cdot \mathbf{n}_\sigma^E \quad \text{and} \quad N_\sigma^{-1} = \sum_{E, \sigma \in E} (K_\sigma^E)^+. \quad (9c)$$

Consistency is obvious. From [1], one can see that the matrix N_σ exists for a symmetrizable system. A slightly different version is

$$\Phi_\sigma^E(\mathbf{u}) = N_\sigma \text{sign}(K_\sigma^E) \mathbf{J}(\mathbf{u}_\sigma) \cdot \nabla \mathbf{u}(\sigma), \quad N_\sigma^{-1} = \sum_{E, \sigma \in E} \text{sign}(K_\sigma^E).$$

The numerical results are identical, and we will use the version (9c).

3.2 Low order schemes

For the average value, one can simply take a standard finite volume (so we do not use the boundary values). We have taken the Lax-Friedrichs numerical flux and the Roe scheme in our simulations.

The real problem is what to do with the point values. A first-order version can be defined as follows. We first, and temporarily for the definition of sub-elements only, re-number the boundary nodes. We pick one degree of freedom, call it b_1 , and list the others in a counter-clockwise manner: we get the list $\{b_1, \dots, b_{N-1}\}$ of all boundary degrees of freedom. The centroid is denoted by b_N , with $N = 7$ for the quadratic approximation, and $N = 10$ for the cubic one. Then we define the sub-elements of vertices $\{b_i, b_N, b_{i+1}\}_{i=1, \dots, N-2}$ and $\{b_{N-1}, b_N, b_1\}$ with a numbering b_i modulo N . This defines $N - 1$ sub-elements that we denote by T_i^E , then we get inward normals \mathbf{n}_{b_i} . For quadratic elements, and using back the original numbering, this is illustrated in Figure 2. In what follows, we use the original numbering with this geometrical definition of sub-elements.

The update of \mathbf{u}_σ is done with (9a) where Φ_σ^E needs to be modified. We use

$$\Phi_\sigma^E = \frac{1}{|C_\sigma|} \sum_{T_i^E, \sigma \in T_i^E} \Phi_\sigma^{T_i^E}(\mathbf{u}). \quad (10)$$

The residuals will be defined the following, which is done to get monotone first-order residual distribution schemes, see [9, 2] for example. We will use two types of residuals:

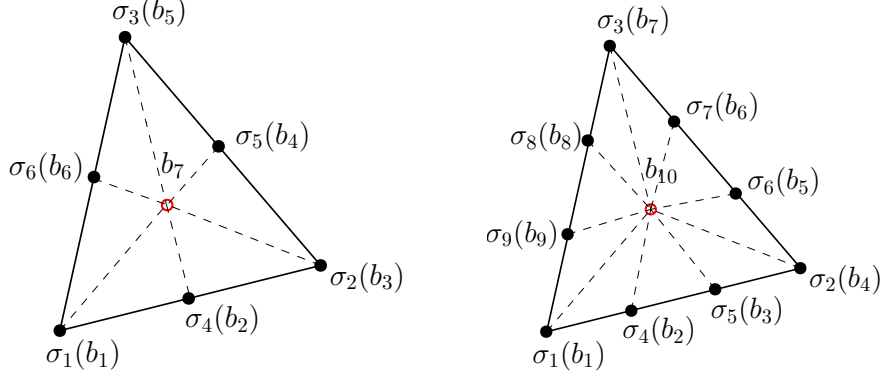


Figure 2: Geometry for the first-order scheme. Left: quadratic; Right: cubic.

- a version that is inspired by the Local Lax-Friedrichs scheme

$$\Phi_{\sigma}^{T_i^E} = \frac{1}{3} \oint_{T_i^E} \mathbf{J}(\mathbf{u}) \cdot \nabla \mathbf{u} \, dx + \alpha_{T_i^E} (\mathbf{u}_{\sigma} - \bar{\mathbf{u}}_{T_i^E})$$

with

$$\oint_{T_i^E} \mathbf{J}(\mathbf{u}) \cdot \nabla \mathbf{u} \, dx \approx |T_i^E| \mathbf{J}(\bar{\mathbf{u}}_{T_i^E}) \nabla \mathbf{u}(\bar{\mathbf{u}}_{T_i^E}), \quad (11)$$

where we use the \mathbb{P}^1 approximation on T_i^E and $\bar{\mathbf{u}}_{T_i^E}$ is the arithmetic average of the \mathbf{u} 's at three vertices of T_i^E (hence we use the average value here). Last,

$$\alpha_{T_i^E} \geq \max_{\substack{\sigma \in T_i^E, \\ \mathbf{n}_{b_i} \text{ normals of } T_i^E}} \rho(\mathbf{J}(\mathbf{u}_{\sigma}) \cdot \mathbf{n}_{b_i}),$$

where $\rho(B)$ is the spectral radius of the matrix B .

- a version that is inspired by the finite volume scheme re-written in the residual distribution framework, see [3] for details. We have used the Roe scheme with Harten-Yee entropy fix.

We still need to define $|C_{\sigma}|$. It is

$$|C_{\sigma}| = \sum_{E, \sigma \in E} \sum_{T_i^E, \sigma \in T_i^E} \frac{|T_i^E|}{3},$$

and after some simple calculations, we see that

$$|C_{\sigma}| = \sum_{E, \sigma \in E} \frac{2|E|}{3(N-1)}.$$

The low-order version can easily be shown to be invariant domain preserving under some CFL conditions. For example, the Local Lax-Friedrichs version needs that

$$3 \frac{\Delta t}{|T_i^E|} \rho(\mathbf{J}(\mathbf{u}_{\sigma}) \cdot \mathbf{n}_{b_i}) \leq 1, \quad \forall E, i$$

and this condition turns out to be much more restrictive than the one we can use in practice.

3.3 Linear stability

Linear stability is not easy to study when the mesh has no particular symmetry, and when the scheme under consideration does not satisfy a variational principle. In the one dimensional case, it is possible to show that the scheme developed in [4] is linearly stable: this has been done by W. Barsukow and reported in [6] using [21]. However, the scheme (9), adapted in 1D, would not be exactly the same as in [4]. So we have conducted an experimental study on several types of meshes generated by GMSH [14] with several types of meshing option (frontal Delaunay, Delaunay). The all proved to be stable for the linear and non-linear problems tested above, with a CFL halved with respect to the standard value for the quadratic approximation and divided by 3 for the cubic approximation. This is more or less what is expected because for the quadratic (resp. cubic) approximation, the density of degrees of freedom is approximately doubled (resp. tripled).

For the first-order approximation, using the Rusanov scheme, it is easy to get a CFL condition under which the solution stays in its domain of dependence.

3.4 Non-linear stabilization

When the solution develops discontinuities, the high-order scheme will be prone to numerical oscillations. To overcome this, we have used a simplified version of the MOOD paradigm in [8, 24]. Since point values and average are independent variables, we need to test both.

The idea is to work with several schemes ranging from order $p = 3$ or 4 to 1, with the lowest order one able to provide results staying in the invariance domain. For the element E , we write the scheme for $\bar{\mathbf{u}}_E$ as $S_E(k)$ and for \mathbf{u}_σ as $S_\sigma(k)$.

We denote by $\bar{\mathbf{u}}_E^n$ and \mathbf{u}_σ^n the solution at the time t_n . After each Runge-Kutta cycle, the updated solution is denoted by $\tilde{\mathbf{u}}_E$, $\tilde{\mathbf{u}}_\sigma$.

We first run the full order scheme, for each Runge-Kutta cycle. Concerning the average $\bar{\mathbf{u}}_E$, we store the flux $\int_\Gamma \mathbf{f}(\mathbf{u}^h) \cdot \mathbf{n}$ for reasons of conservation. Then, for the average,

1. Computer Admissible Detector (CAD in short): We check if $\tilde{\mathbf{u}}_E$ is a valid vector with real components: we check if each component is not NaN. Else, we flag the element and go to the next one in the list.
2. Physically Admissible Detector (PAD in short): We check if $\tilde{\mathbf{u}}_E \in \mathcal{D}$. If this is false, the element is flagged, and go to the next one in the list.
3. Then we check if at t_n , the solution is not a constant in the elements used in the numerical stencil (so we check and compare between the average $\bar{\mathbf{u}}_E$ and point values \mathbf{u}_σ in E with these in the elements sharing a face with E). This is done in order to avoid to detect a fake maximum principle. If the solution is declared locally constant, we move to the next element.
4. Discrete Maximum Principle (DMP in short): we check if $\tilde{\mathbf{u}}_E$ is a local extrema. if we are dealing with the Euler equations, we compute the density and the pressure and perform this test on these two values only, even though for a system this is not really meaningful. We denote by ξ the functional on which we perform the test (i.e., \mathbf{u} itself for scalar problems, and the density/pressure obtained from $V(E)$: the set of elements that share a face or a vertex with E , excluding E itself). We say we have a potential extrema if

$$\xi_E^{n+1} \notin [(\min_{F \in V(E)} \xi_F^n) - \varepsilon_E^n, (\max_{F \in V(E)} \xi_F^n) + \varepsilon_E^n],$$

where ε_E^n is estimated as in [8]. If the test is wrong, we go to the next element, else the element is flagged.

If an element is flagged, then each of its faces are flagged, and re-compute the flux of the flagged faces using the first-order scheme.

For the point values, the procedure is similar, and then for the flagged degrees of freedom, we re-compute $\sum_{E, \sigma \in E} \Phi_\sigma^E(\mathbf{u}^n)$ with the first-order scheme.

4 Numerical results

In this section, we demonstrate the performance of the developed schemes in §3 on several numerical examples. When MOOD is activated, we use the local Rusanov scheme (with a small stencil) as described in §3.2. The CFL number (based on the elements) is always set to 0.4.

4.1 Scalar case

We begin with the scalar case,

$$\frac{\partial u}{\partial t} + \mathbf{a}(\mathbf{x}) \cdot \nabla u = 0, \quad (12)$$

with, for $\mathbf{x} = (x, y)$, $\mathbf{a}(\mathbf{x}) = (a^{(1)}, a^{(2)})$ representing the velocity field that the quantity u is moving with.

4.1.1 Convection problem

In the first example, we consider $\mathbf{a}(\mathbf{x}) = 2\pi(- (y - y_0), x - x_0)$ and note that $\operatorname{div} \mathbf{a} = 0$, so that (12) can be put in a conservative form. The domain is $\Omega = [-20, 20]^2$, $(x_0, y_0) = (0, 0)$ and the initial condition is

$$u_0(\mathbf{x}) = e^{-\|\mathbf{x} - \tilde{\mathbf{x}}_0\|^2}, \quad \tilde{\mathbf{x}}_0 = (5, 5). \quad (13)$$

The solution is checked after one rotation ($T = 1$) with the exact one. The initial mesh is obtained with GMSH, using the front Delaunay option. Then we sub-divide the mesh by cutting the edges into two equal or three equal segments, and a quadratic approximation or a cubic approximation is employed. The discrete L^1 -, L^2 -, and L^∞ -errors of the point values u computed with quadratic and cubic approximations are shown in Tables 1 and 2, respectively. As one can clearly see that, the expected third- and fourth-order accuracy are achieved.

Table 1: Errors and rates on the point values for the initial condition (13) with the quadratic approximation of (6)-(9).

h	L^1	rate	L^2	rate	L^∞	rate
2.00×10^{-1}	4.309×10^{-1}	-	6.703×10^{-2}	-	3.270×10^{-2}	-
1.91×10^{-1}	3.749×10^{-1}	2.85	5.857×10^{-2}	2.77	2.871×10^{-2}	2.66
1.82×10^{-1}	3.241×10^{-1}	3.13	5.079×10^{-2}	3.06	2.512×10^{-2}	2.87
1.74×10^{-1}	2.850×10^{-1}	2.89	4.485×10^{-2}	2.80	2.215×10^{-2}	2.83
1.67×10^{-1}	2.553×10^{-1}	2.59	4.026×10^{-2}	2.54	2.007×10^{-2}	2.39
1.60×10^{-1}	2.269×10^{-1}	2.89	3.584×10^{-2}	2.84	1.786×10^{-2}	2.78
1.33×10^{-1}	1.317×10^{-1}	2.98	2.100×10^{-2}	2.93	1.056×10^{-2}	2.88

4.1.2 Zalesak test case

In the second example, we consider a Zalesak's problem, which involves the solid body rotation of a notched disk. Here the domain is $[0, 1]^2$ and the rotation field is $\mathbf{a}(\mathbf{x})$ also defined to be a rotation with respect to $(x_0, y_0) = (0.5, 0.5)$ and angular speed of 2π . The initial condition is

$$u_0(\mathbf{x}) = \begin{cases} 0.25(1 + \cos(\frac{\pi r_1}{0.15})) & \text{if } r_1 = \|\mathbf{x} - (0.25, 0.5)\| \leq 0.15, \\ 1 - \frac{r_2}{0.15} & \text{if } r_2 = \|\mathbf{x} - (0.5, 0.25)\| \leq 0.15, \\ 1 & \text{if } r_3 = \|\mathbf{x} - (0.5, 0.75)\| \leq 0.15, \\ 0 & \text{if } |x - 0.5| \leq 0.025 \text{ and } y \in [0.6, 0.85]. \end{cases}$$

Table 2: Errors and rates on the point values for the initial condition (13) with the cubic approximation of (6)-(9).

h	L^1	rate	L^2	rate	L^∞	rate
4.00×10^{-1}	5.219×10^{-1}	-	6.800×10^{-2}	-	2.206×10^{-2}	-
3.33×10^{-1}	2.440×10^{-1}	4.17	3.268×10^{-2}	4.02	1.121×10^{-2}	3.71
2.86×10^{-1}	1.358×10^{-1}	3.80	1.839×10^{-2}	3.73	6.339×10^{-3}	3.70
2.50×10^{-1}	7.978×10^{-2}	3.99	1.083×10^{-2}	3.96	3.705×10^{-3}	4.02
2.22×10^{-1}	4.868×10^{-2}	4.19	6.634×10^{-3}	4.16	2.321×10^{-3}	3.97
2.00×10^{-1}	3.267×10^{-2}	4.19	4.458×10^{-3}	4.16	1.542×10^{-3}	3.97

We use the MOOD procedure and compute the numerical solution with a mesh that has 3442 vertices, 10123 edges, and 16881 elements (hence 13565 (resp. 40569) DoFs in total for the quadratic (resp. cubic) approximation, thanks to the Euler relation). The results computed by the quadratic approximation after 1, 2, and 3 rotations are displayed in Figures 3–4. From the sub-plots in the first two columns of these figures,

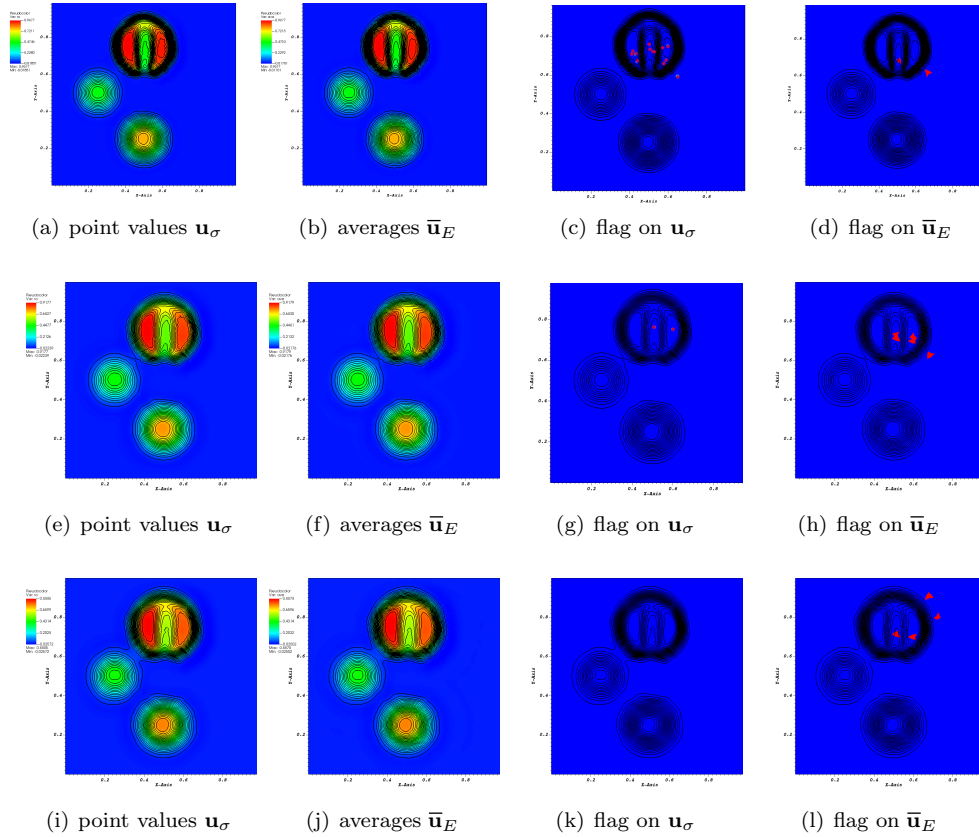


Figure 3: Zalesak problem: quadratic approximation and MOOD criteria are checked expect for PAD. Top row: $T = 1$; Middle row: $T = 2$; Bottom row: $T = 3$.

one can observe that, both the point values and the average values can be correctly captured. In the last two columns of these figures, we also indicate in red where the MOOD criteria are violated. We first check the criteria expect for PAD. From the sub-plots in the last two columns of Figure 3, we see that, as expected,

the first-order scheme is only used around the region where the solution is non-smooth. We also observe that the minimum values of \mathbf{u}_σ and $\bar{\mathbf{u}}_E$ are $\approx -10^{-2}$. This is due to the fact that the PAD is not checked.

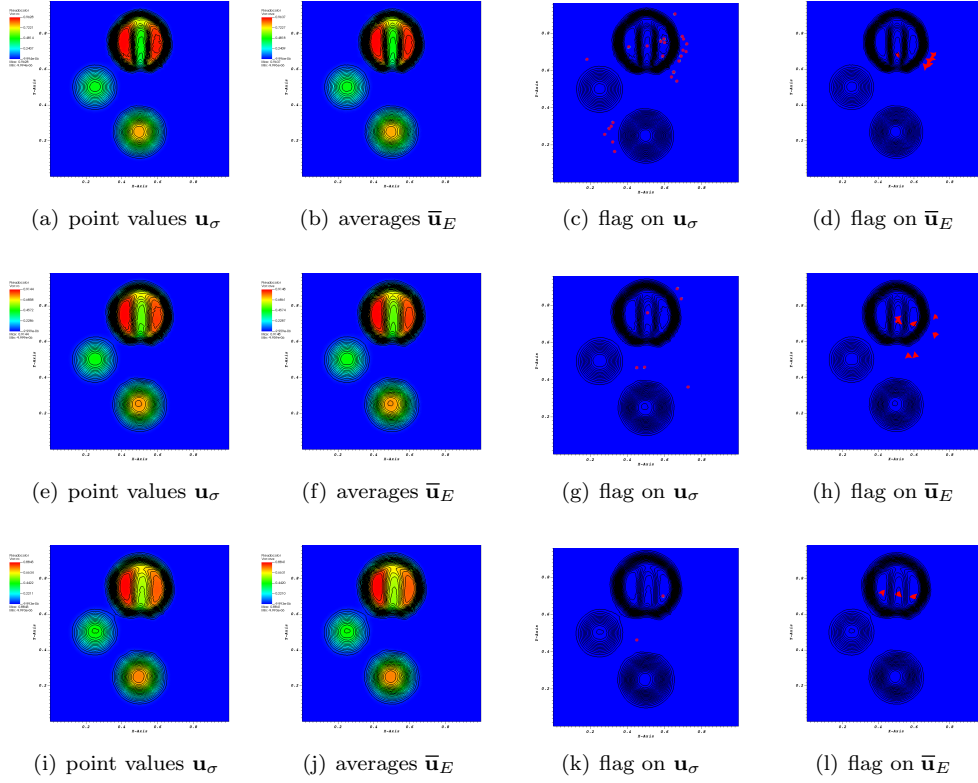


Figure 4: Zalesak problem: quadratic approximation and all MOOD criteria are checked. Top row: $T = 1$; Middle row: $T = 2$; Bottom row: $T = 3$.

We then check all the MOOD criteria including PAD, and say that PAD is violated if $\mathbf{u}_\sigma < -10^{-5}$ or $\bar{\mathbf{u}}_E < -10^{-5}$. From the sub-plots in the last two columns of Figure 4, we clearly see that the first-order scheme will be also used in the region where the solution is smooth but PAD may not be satisfied. At the same time, we can see that the minimum values of \mathbf{u}_σ and $\bar{\mathbf{u}}_E$ are $> -10^{-5}$, which satisfy the assumed PAD criterion.

Finally, we compute the solutions using the cubic approximation. For saving space, only the results obtained with all MOOD criteria checked are presented in Figure 5. Comparing the sensor results with these computed by the quadratic approximation, we observe that the cubic approximation leads to less activation of the MOOD paradigm.

4.1.3 KPP test case

In the third example, we consider the KPP problem which has been first considered by Kurganov, Popov and Petrova in [18]. The governing PDE is

$$\frac{\partial u}{\partial t} + \frac{\partial(\sin u)}{\partial x} + \frac{\partial(\cos u)}{\partial y} = 0, \quad (14)$$

in a domain $[-2, 2]^2$ with the initial condition

$$u_0(\mathbf{x}) = \begin{cases} \frac{7}{2}\pi & \text{if } \|\mathbf{x} - (0, 0.5)\|^2 \leq 1, \\ \frac{\pi}{4} & \text{else.} \end{cases}$$

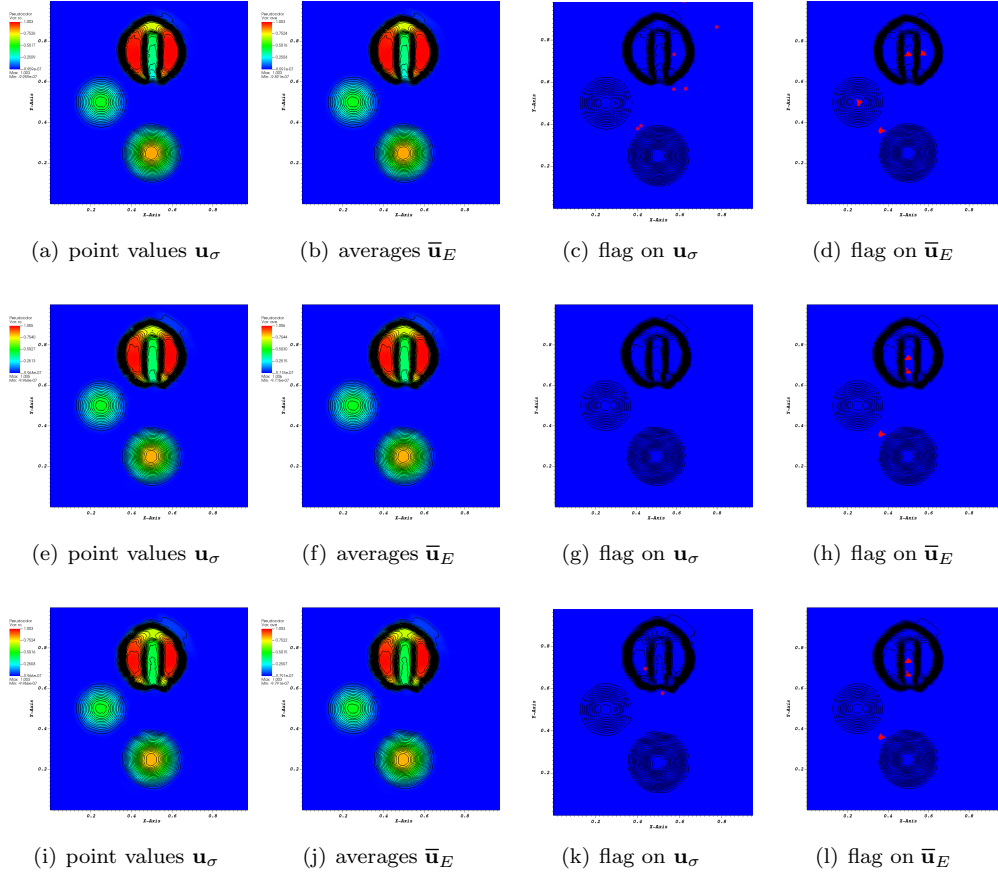


Figure 5: Zalesak problem: cubic approximation and all MOOD criteria are checked. Top row: $T = 1$; Middle row: $T = 2$; Bottom row: $T = 3$.

The problem (14) is non-convex, in the sense that compound wave may exist. Here we have used the MOOD paradigm with the Local Lax-Friedrichs scheme as a first-order scheme. We compute the numerical solutions until the final time $T = 1$ using both the quadratic and cubic approximations. For the quadratic (resp. cubic) approximation, the mesh has 8601 vertices, 25480 edges, 16880 elements, and 34081 (resp. 76441) degrees of freedom. We present the obtained numerical results in Figures 6 and 7.

If the method is not dissipative enough, the two shocks in the northwest direction at around 22° will be attached which is not correct. Here this is not the case, and the solution looks correct, at least in comparison with the existing literature on the subject. We are not aware of any form of exact analytical solution. We also indicate in red where the computed quantities (\mathbf{u}_σ or $\bar{\mathbf{u}}_E$) violate MOOD criteria (PAD is included) given in §3.4. As one can see, the low-order scheme is only activated at a limited number of locations. When the cubic approximation is used, the average values do not violate the MOOD criteria at the final time.

4.2 Euler equations

We proceed with Euler equations of gas dynamics and consider the following six cases:

- a stationary vortex case in $[-10, 10]^2$ for $T = 3$.
- a moving vortex case in $[-20, 20]^2$ for $T = 20$.
- the Sod problem in $[-1, 1]^2$ for $T = 0.16$.

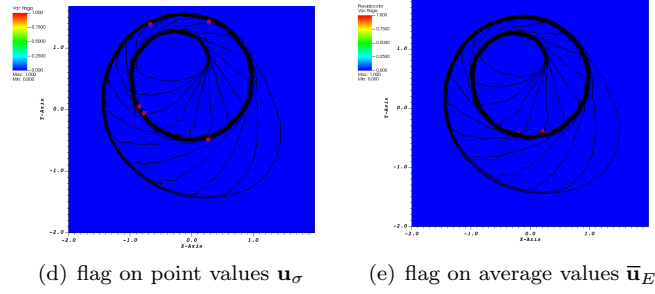
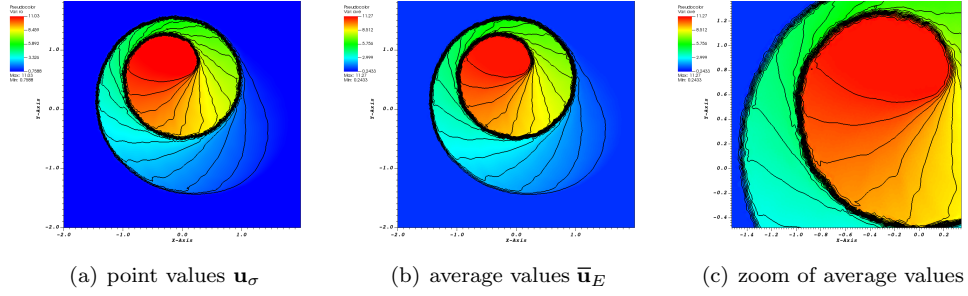


Figure 6: KPP problem: using quadratic approximation.

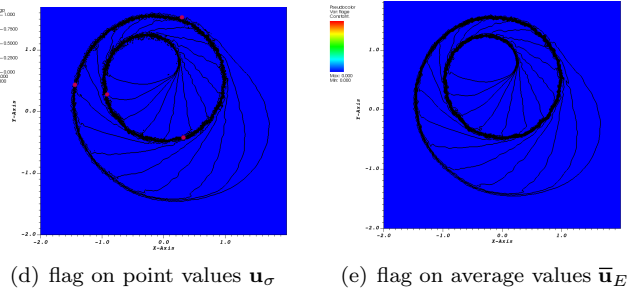
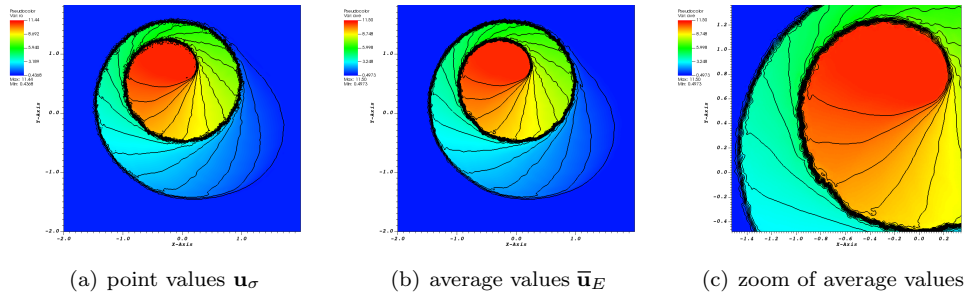


Figure 7: KPP problem: using cubic approximation.

- the 13th case studied by Liu and Lax [20], where the solution is shown at time $T = 1$.
- the 3rd case of [19] by Kurganov and Tadmor for $T = 1$.
- the double Mach reflection case of Woodward and Collela, [26].

4.2.1 Accuracy test

In the first example of non-linear system cases, we verify the order of convergence of the proposed scheme. To this end, we consider a smooth stationary isentropic vortex flow. The computational domain is $[-10, 10] \times [-10, 10]$ with Dirichlet boundary conditions everywhere. The initial condition is given by

$$\rho = (1 + \delta T)^{\frac{1}{\gamma-1}}, \quad u = -\frac{\varepsilon}{2\pi} x_2 e^{\frac{1-r^2}{2}}, \quad v = \frac{\varepsilon}{2\pi} x_1 e^{\frac{1-r^2}{2}}, \quad p = \rho^\gamma, \quad (15)$$

where the vortex strength is $\varepsilon = 5$ and $\delta T = -\frac{(\gamma-1)\varepsilon^2}{8\gamma\pi^2} e^{1-r^2}$ with $r = \|\mathbf{x}\| = \sqrt{x_1^2 + x_2^2}$. This is a stationary equilibrium of the system so the exact solution coincides with the initial condition at any time. The proposed scheme is not able to exactly preserve this equilibrium state and the truncation error is $\mathcal{O}(h^p)$, where h is the characteristic size of the triangular mesh and p is the order of the scheme. Thus, it serves as a good numerical example to verify the order of convergence, see also, e.g. in [13, 5].

Tables 3–6 report the convergence rates of quadratic and cubic approximations for the vortex test problem run on a sequence of successively refined meshes. The meshes are obtained from the Cartesian 40×40 , 80×80 , 160×160 , 320×320 , and 640×640 meshes which are all cut by the diagonal. From the obtained results, we can clearly see that the expected third- and fourth-accuracy are achieved by the proposed schemes with quadratic and cubic approximations, respectively.

Table 3: Errors and rates on the average values of density, quadratic approximation, $T = 3$.

h	L^1	rate	L^2	rate	L^∞	rate
3.6262×10^{-1}	1.262×10^{-4}	-	2.850×10^{-5}	-	8.406×10^{-3}	-
1.7901×10^{-1}	2.220×10^{-5}	2.46	4.851×10^{-6}	2.51	1.364×10^{-3}	2.58
8.8944×10^{-2}	3.179×10^{-6}	2.78	6.865×10^{-7}	2.80	2.058×10^{-4}	2.70
4.4332×10^{-2}	4.172×10^{-7}	2.92	9.093×10^{-8}	2.90	2.843×10^{-5}	2.84
2.2132×10^{-2}	5.298×10^{-8}	2.97	1.160×10^{-8}	2.96	3.660×10^{-6}	2.95

Table 4: Errors and rates on the point values of density, quadratic approximation, $T = 3$.

h	L^1	rate	L^2	rate	L^∞	rate
2.9608×10^{-1}	9.100×10^{-5}	-	2.696×10^{-5}	-	1.979×10^{-2}	-
1.4616×10^{-1}	1.526×10^{-5}	2.53	4.083×10^{-6}	2.68	1.960×10^{-3}	3.28
7.2623×10^{-2}	2.182×10^{-6}	2.78	5.799×10^{-7}	2.79	2.355×10^{-4}	3.03
3.6198×10^{-2}	2.860×10^{-7}	2.92	7.685×10^{-8}	2.90	3.323×10^{-5}	2.81
1.8070×10^{-2}	3.630×10^{-8}	2.97	9.796×10^{-9}	2.96	4.356×10^{-6}	2.92

Table 5: Errors and rates on the average values of density, cubic approximation, $T = 3$.

h	L^1	rate	L^2	rate	L^∞	rate
3.6262×10^{-1}	1.956×10^{-5}	-	4.651×10^{-6}	-	2.051×10^{-3}	-
1.7901×10^{-1}	8.975×10^{-7}	4.37	1.603×10^{-7}	4.77	5.134×10^{-5}	5.22
8.8944×10^{-2}	4.970×10^{-8}	4.14	8.579×10^{-9}	4.19	3.373×10^{-6}	3.89
4.4332×10^{-2}	1.867×10^{-7}	4.08	4.829×10^{-10}	4.13	2.895×10^{-9}	4.16
2.2132×10^{-2}	1.755×10^{-10}	4.03	2.863×10^{-11}	4.07	1.128×10^{-8}	4.04

Table 6: Errors and rates on the point values of density, cubic approximation, $T = 3$.

h	L^1	rate	L^2	rate	L^∞	rate
2.4175×10^{-1}	1.462×10^{-5}	-	4.990×10^{-6}	-	2.169×10^{-3}	-
1.1934×10^{-1}	6.647×10^{-7}	4.38	1.713×10^{-7}	4.78	9.512×10^{-5}	4.43
5.9296×10^{-2}	3.733×10^{-8}	4.12	9.757×10^{-9}	4.10	5.200×10^{-6}	4.16
2.9555×10^{-2}	2.253×10^{-9}	4.03	5.953×10^{-10}	4.02	3.018×10^{-7}	4.09
1.4754×10^{-2}	1.399×10^{-10}	4.00	3.798×10^{-11}	3.96	2.254×10^{-8}	3.73

4.2.2 Moving vortex problem

In the second example of non-linear system cases, we consider the following initial condition:

$$\rho = (T_\infty + \Delta T)^{\frac{1}{\gamma-1}}, \quad u = u_\infty - y_2 M e^{\frac{1-R}{2}}, \quad v = v_\infty + y_1 M e^{\frac{1-R}{2}}, \quad p = \rho^\gamma, \quad (16)$$

prescribed in the domain $[-20, 20]^2$. In (16), $(u_\infty, v_\infty) = (1, \frac{\sqrt{2}}{2})$, $T_\infty = 1$, $M = \frac{5}{2\pi}$, $\mathbf{y} = (\mathbf{x} - \mathbf{x}_0)/2$ with $\mathbf{x}_0 = (-10, -10)$, $R = \|\mathbf{y}\|^2$, and $\Delta T = -\frac{\gamma-1}{2\gamma} M^2 e^{1-R}$. This vortex is simply advected with the velocity (u_∞, v_∞) so that it is very easy to compute the exact solution. The third- and fourth-order results at the final time $T = 20$, for the scheme (6)-(9), are shown in Figures 8 and 9. The mesh as a comparison with the exact solution is also shown. We have also displayed zooms of the solutions at $T = 20$, superimposed with the exact one. For the fourth-order case, it is difficult to see a difference, at this scale, between the exact and numerical solutions. In the two cases, the mesh that is plotted is obtained from the actual computational mesh where we have sub-divided the elements using the Lagrange points: these meshes represent all the degrees of freedom that we actually use. It turns out that the plotting meshes (represented) are identical for the two types of solutions.

4.2.3 2D Sod problem

In the third example of non-linear system cases, we test the proposed schemes on a well-known 2D Sod benchmark problem. The initial condition is given by

$$(\rho, u, v, p) = \begin{cases} (1, 0, 0, 1.5) & \text{if } \|\mathbf{x}\|^2 \leq 0.25, \\ (0.125, 0, 0, 0.1) & \text{else,} \end{cases}$$

the boundary condition is solid wall, and the final time we compute is $T = 0.16$. The two approximations (quadratic and cubic) have been used to compute the solutions. We plot the results (density component) in Figure 10. As one can see, both two approximations produce similar results and cubic approximation is much more accurate as expected. In Figure 11, we also plot the flags where the first-order scheme is activated at the final time. We can clearly see that only the first-order scheme for the point values is used and the cubic approximation leads to less triggers of the first-order scheme.

4.2.4 Liu-Lax problem

In the fourth example of non-linear system cases, we consider the following initial condition

$$(\rho, u, v, p) = \begin{cases} (\rho_1, u_1, v_1, p_1) = (0.5313, 0, 0, 0.4) & \text{if } x \geq 0 \text{ and } y \geq 0, \\ (\rho_2, u_2, v_2, p_2) = (1, 0.7276, 0, 1) & \text{if } x \leq 0 \text{ and } y \geq 0, \\ (\rho_3, u_3, v_3, p_3) = (0.8, 0, 0, 1) & \text{if } x \leq 0 \text{ and } y \leq 0, \\ (\rho_4, u_4, v_4, p_4) = (1, 0, 0.7276, 1) & \text{if } x \geq 0 \text{ and } y \leq 0, \end{cases}$$

prescribed in the computational domain $[-2, 2]^2$. The states 1 and 2 are separated by a shock. The states 2 and 3 are separated by a slip line. The states 3 and 4 are separated by a steady slip-line. The states 4

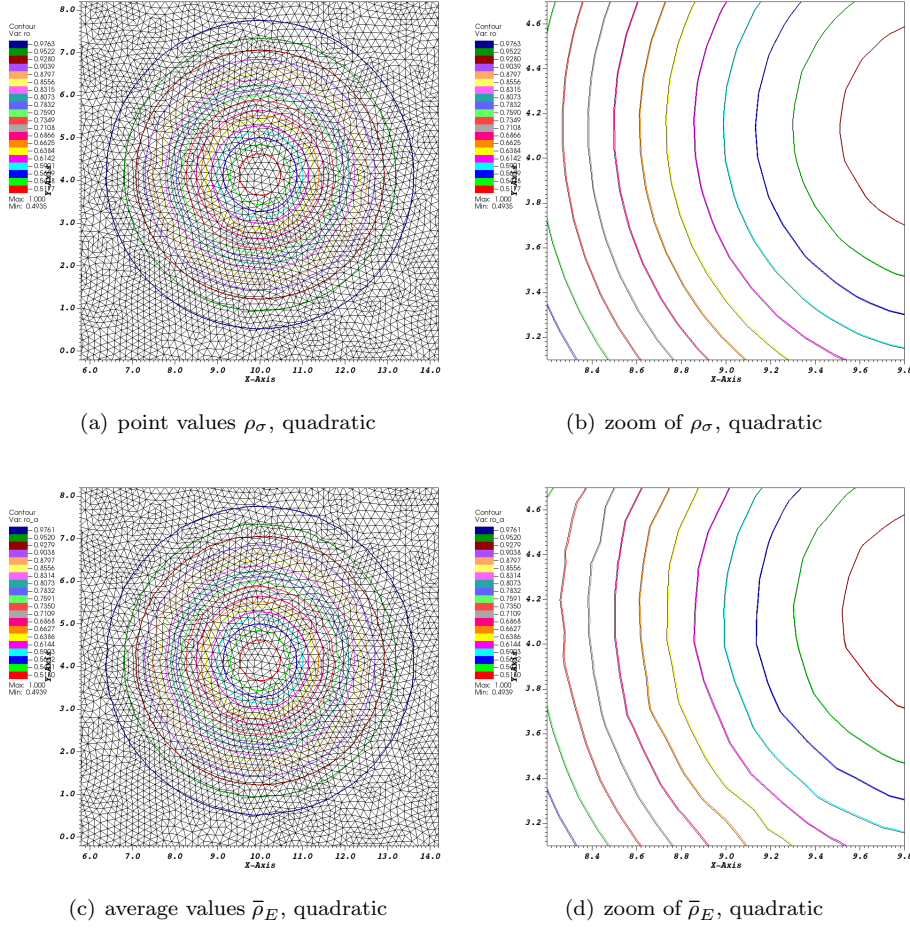


Figure 8: Moving vortex problem: density, zoom of the solution and the mesh. The exact solution is in black lines, the numerical solution with colored isolines. The mesh has 69705 DoFs, 35082 elements, third-order scheme.

and 1 are separated by a shock. The mesh has 53227 vertices, 158878 edges, 105652 elements, and 212105 (resp. 476635) DoFs for the quadratic (resp. cubic) approximation. The obtained results of density field are plotted in Figure 12.

4.2.5 Kurganov-Tadmor problem

In the fifth example of non-linear system cases, the initial condition is

$$(\rho, u, v, p) = \begin{cases} (\rho_1, u_1, v_1, p_1) = (1.5, 0, 0, 1.5) & \text{if } x \geq 1 \text{ and } y \geq 1, \\ (\rho_2, u_2, v_2, p_2) = (0.5323, 1.206, 0, 0.3) & \text{if } x \leq 1 \text{ and } y \geq 1, \\ (\rho_3, u_3, v_3, p_3) = (0.138, 1.206, 1.206, 0.029) & \text{if } x \leq 1 \text{ and } y \leq 1, \\ (\rho_4, u_4, v_4, p_4) = (0.5323, 0, 1.206, 0.3) & \text{if } x \leq 1 \text{ and } y \leq 1. \end{cases}$$

Here the four states are separated by shocks. The domain is $[0, 1.2]^2$. The solution at $T = 1$ is displayed in Figure 13. The mesh has 53140 vertices, 158617 edges, 105478 elements, and 211757 (resp. 475852) DoFs for the quadratic (resp. cubic) approximation. We see that, on the one hand, the solution looks very similar to what was obtained in the literature, see e.g. in [17, 15, 25]. On the other hand, the first-order schemes (for average and point values) are activated on very few positions, see Figure 14.

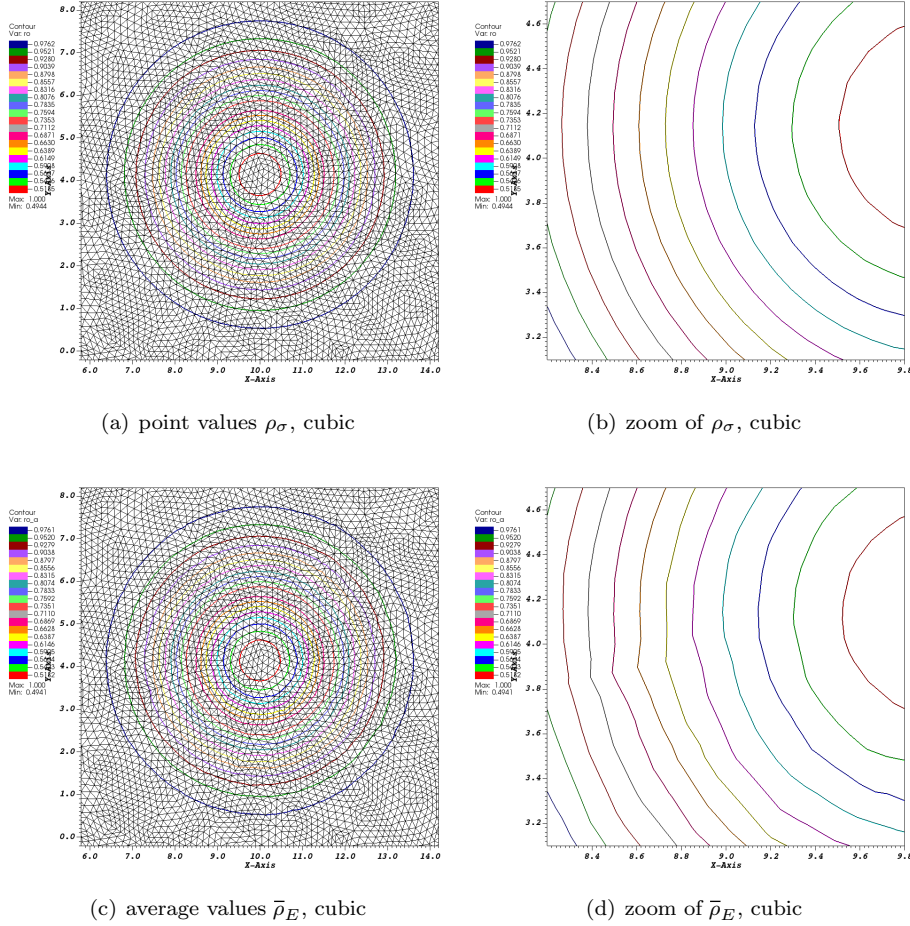


Figure 9: Moving vortex problem: density, zoom of the solution and the mesh. The exact solution is in black lines, the numerical solution with colored isolines. The mesh has 70762 DoFs, 15930 elements, fourth-order scheme.

4.2.6 Woodward-Collela problem

In the final example of non-linear system cases, we consider a double Mack reflection problem. The domain is a ramp, and initially a shock at Mach 10 is set at $x = 0$. The mesh has 29290 vertices, 57870 elements and 87159 edges, i.e., 116449 (reps. 261478) DoFs for the quadratic (reps. cubic) approximation. The right condition is

$$(\rho_R, u_R, v_R, p_R) = (\gamma, 0, 0, 1),$$

so that the speed of sound is 1 ($\gamma = 1.4$) and the left state is obtained assuming a shock at Mach 10, so that

$$(\rho_L, u_L, v_L, p_L) = (8, 8.25, 0, 116.5).$$

The solution at $T = 0.2$ is shown on Figure 15. We observe slight oscillations in the numerical solution, indicating the need for carefully designing limiting strategies or adjusting the MOOD criteria. This will be a focus of our future research. We also display the locations where the first-order scheme is activated at the final time, see Figure 16.

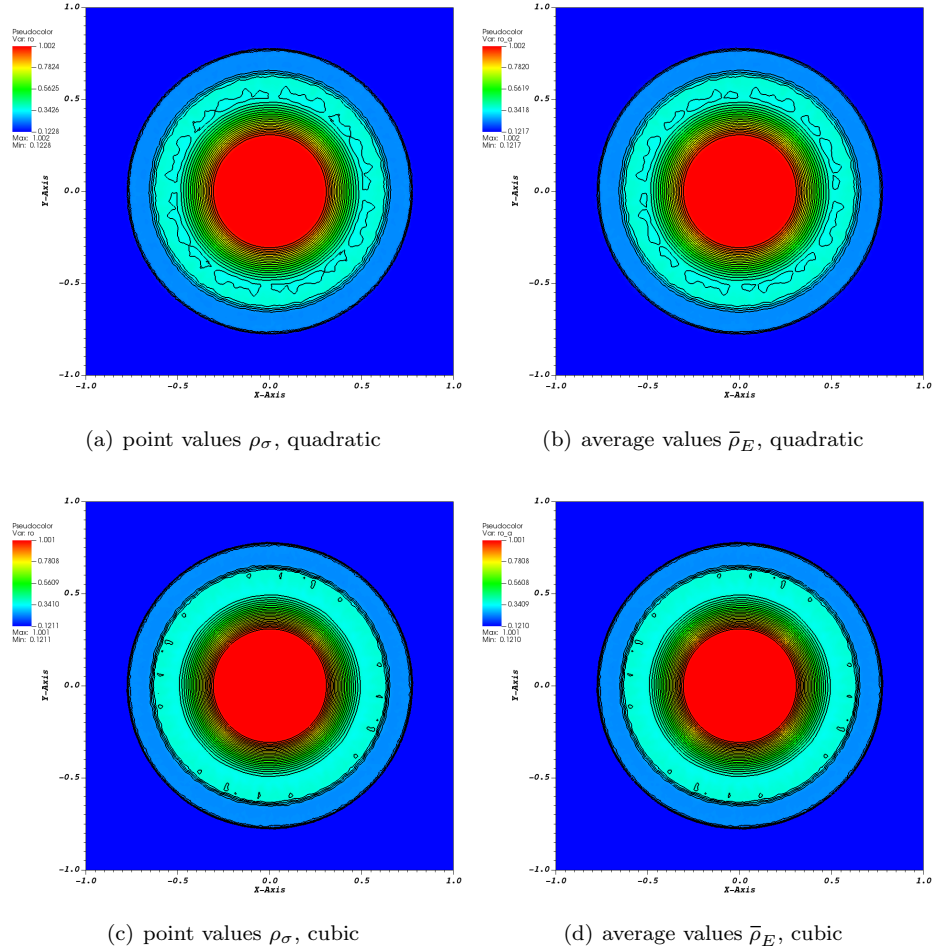


Figure 10: Sod problem: profiles of density.

5 Conclusions

We have presented a computational method inspired by the so-called Active Flux method, following the ideas developed in [4] and [6], and using triangular type meshes. The method is able to capture shocks. We have illustrated the behavior of this method on several cases with smooth and discontinuous problems and models ranging from scalar to systems. The behavior of the method is as expected.

A Boundary conditions for the Euler equations

We have considered two type of boundary condition on $\partial\Omega$ where $\Omega \subset \mathbb{R}^2$: wall boundary conditions and inflow/outflow. We describe how they are implemented for the update of the average values and the point values.

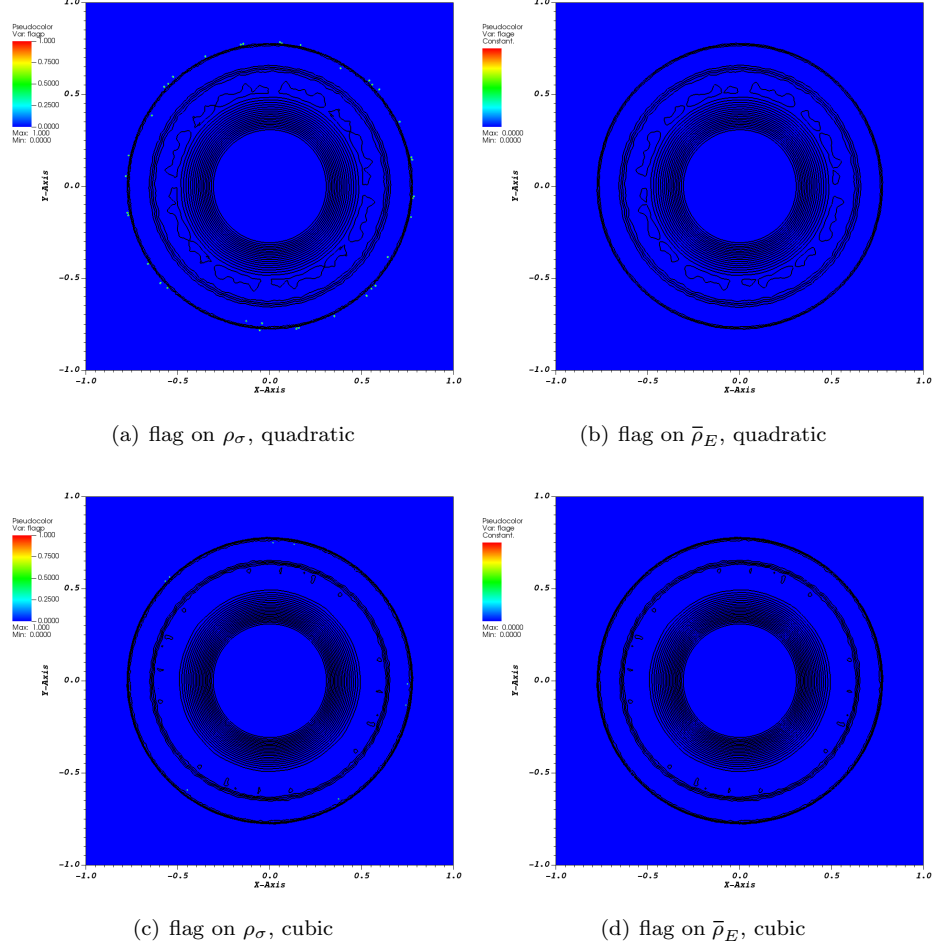


Figure 11: Sod problem: flags at the positions where the first-order scheme is used.

A.1 Average values

Inside the domain, $\bar{\mathbf{u}}_E$ will satisfy:

$$|E| \frac{d\bar{\mathbf{u}}_E}{dt} + \oint_{\partial E} \hat{\mathbf{f}}_{\mathbf{n}}(\mathbf{u}^h, \mathbf{u}^-) d\ell = |E| \frac{d\bar{\mathbf{u}}_E}{dt} + \sum_{\Gamma, \text{edge of } E} \int_{\Gamma} \hat{\mathbf{f}}_{\mathbf{n}}(\mathbf{u}^h, \mathbf{u}^-) d\Gamma = 0,$$

where the numerical flux is the continuous one for the high-order scheme and a standard numerical flux for the first-order case. Here, \mathbf{u}^h is the value of \mathbf{u} on the boundary of ∂E , \mathbf{u}^- is the value on the opposite side of the element, and \mathbf{n} is the local normal.

If one edge Γ is contained in $\partial\Omega$, we modify

$$\int_{\Gamma} \hat{\mathbf{f}}_{\mathbf{n}}(\mathbf{u}^h, \mathbf{u}^-) d\ell \approx |\Gamma| \sum_{\text{quadrature points}} \omega_q \hat{\mathbf{f}}_{\mathbf{n}}(\mathbf{u}^h(\mathbf{x}_q), \mathbf{u}^-(\mathbf{x}_q))$$

evaluated by a quadrature rule. We use a Gaussian quadrature with 3 points. The following cases are considered:

- for wall, by setting the state $\mathbf{u}^-(\mathbf{x}_q)$ equal to the state obtained from $\mathbf{u}^h(\mathbf{x}_q)$ by symmetry with respect

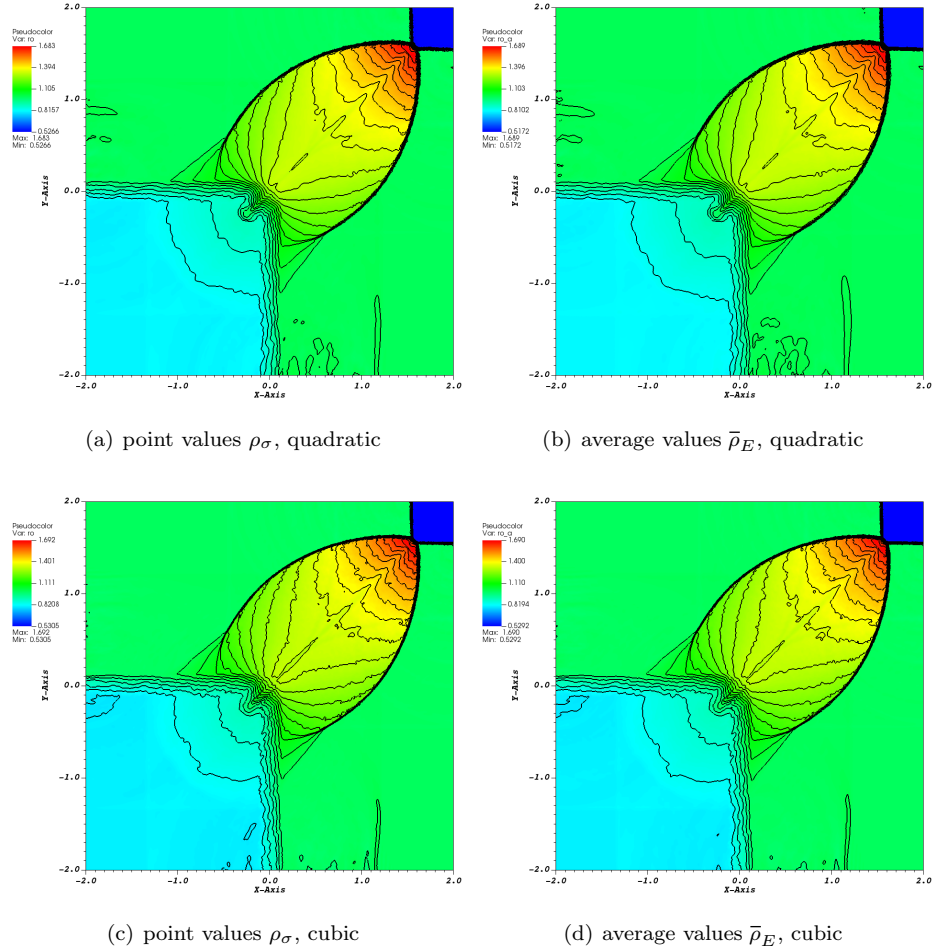


Figure 12: Liu-Lax case: profiles of density.

to Γ , i.e., same density, same pressure, but the velocity \mathbf{v} is

$$\mathbf{v}^-(\mathbf{x}_q) = \mathbf{v}^h(\mathbf{x}_q) - 2 \frac{\langle \mathbf{v}^h(\mathbf{x}_q), \mathbf{n} \rangle}{\|\mathbf{n}\|^2} \mathbf{n}.$$

- for inflow/outflow, since we want to impose $\mathbf{u} = \mathbf{u}_\infty$ weakly, we take $\mathbf{u}^- = \mathbf{u}_\infty$, and the flux is some upwind flux (the Roe one for the numerical experiments).
- for supersonic inflow/outflows or if the solution stays constant in a neighborhood of the boundary, we will impose Neumann condition, i.e., we force the solution to stay constant.

A.2 Point values

It is a bit more involved. Let us remind that the update of the point values is made by (9a)

$$\frac{d\mathbf{u}_\sigma}{dt} + \sum_{E, \sigma \in E} \Phi_\sigma^E(\mathbf{u}) = 0, \quad (17)$$

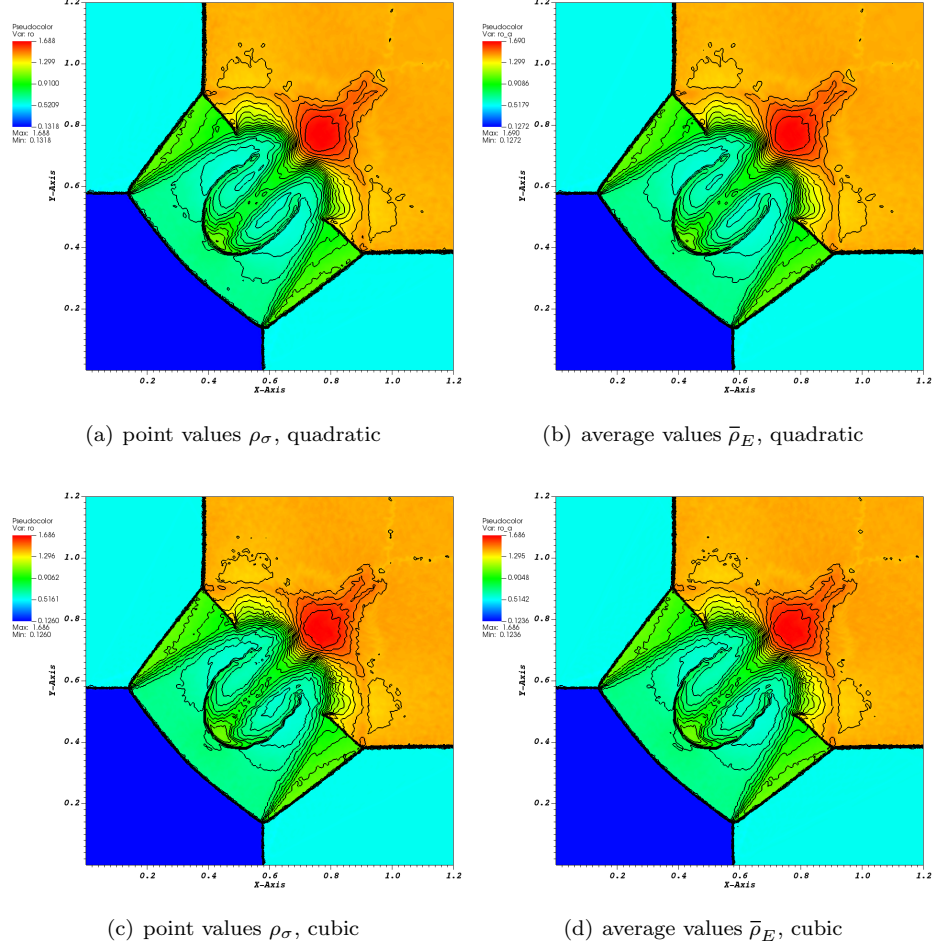


Figure 13: Kurganov-Tadmor problem: profiles of density.

that we have to modify into

$$\frac{d\mathbf{u}_\sigma}{dt} + \sum_{E, \sigma \in E} \Phi_\sigma^E(\mathbf{u}) + \sum_{\Gamma \subset \partial\Omega, \sigma \in \Gamma} \Phi_\sigma^\Gamma(\mathbf{u}) = 0, \quad (18)$$

and we need to define $\Phi_\sigma^\Gamma(\mathbf{u})$. We do it in two cases:

- Neumann condition: again, we force the solution to stay the same, i.e.,

$$\sum_{E, \sigma \in E} \Phi_\sigma^E(\mathbf{u}) + \sum_{\Gamma \subset \partial\Omega, \sigma \in \Gamma} \Phi_\sigma^\Gamma(\mathbf{u}) = 0.$$

In practice, once $\sum_{E, \sigma \in E} \Phi_\sigma^E(\mathbf{u})$ in (17) has been computed, we set this quantity to 0.

- wall. For each Γ in (18), with normal \mathbf{n} , there is one element E that has Γ as one of its edges. Then we consider E^- , the (virtual) element that is symmetric with respect to \mathbf{n} . We consider \mathbf{u}^- , the state symmetric to \mathbf{u}^h with respect to \mathbf{n} , i.e., same density and pressure, and symmetric velocity. By this we define $\Phi_\sigma^\Gamma(\mathbf{u}^h)$ by $\Phi_\sigma^\Gamma(\mathbf{u}^h) = \Phi^{E^-}(\mathbf{u}^-)$.

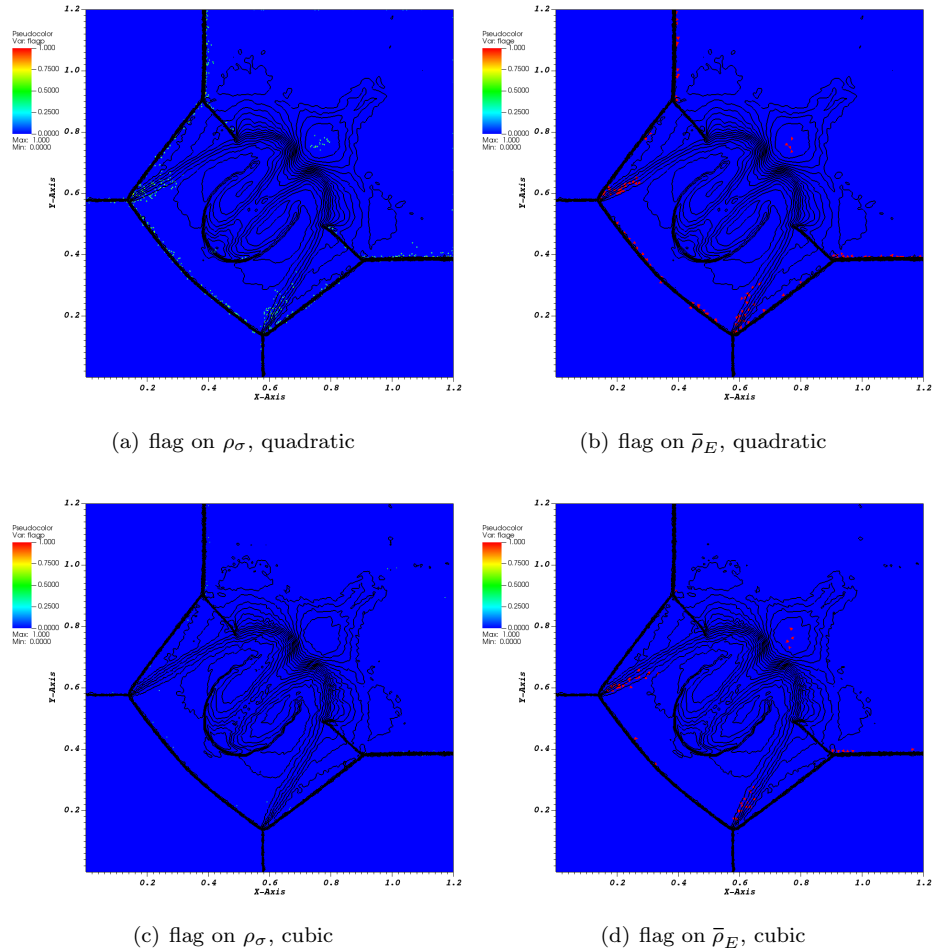


Figure 14: Kurganov-Tadmor problem: flags at the positions where the first-order scheme is used.

References

- [1] R. Abgrall. Toward the ultimate conservative scheme: Following the quest. *J. Comput. Phys.*, 167(2):277–315, 2001.
- [2] R. Abgrall. Essentially non oscillatory residual distribution schemes for hyperbolic problems. *J. Comput. Phys.*, 214(2):773–808, 2006.
- [3] R. Abgrall. Some remarks about conservation for residual distribution schemes. *Comput. Methods Appl. Math.*, 18(3):327–351, 2018.
- [4] R. Abgrall. A combination of residual distribution and the active flux formulations or a new class of schemes that can combine several writings of the same hyperbolic problem: application to the 1d Euler equations. *Commun. Appl. Math. Comput.*, 5(1):370–402, 2023.
- [5] R. Abgrall, P. Bacigaluppi, and S. Tokareva. High-order residual distribution scheme for the time-dependent Euler equations of fluid dynamics. *Computers and Mathematics with Applications*, 78:274–297, 2019.

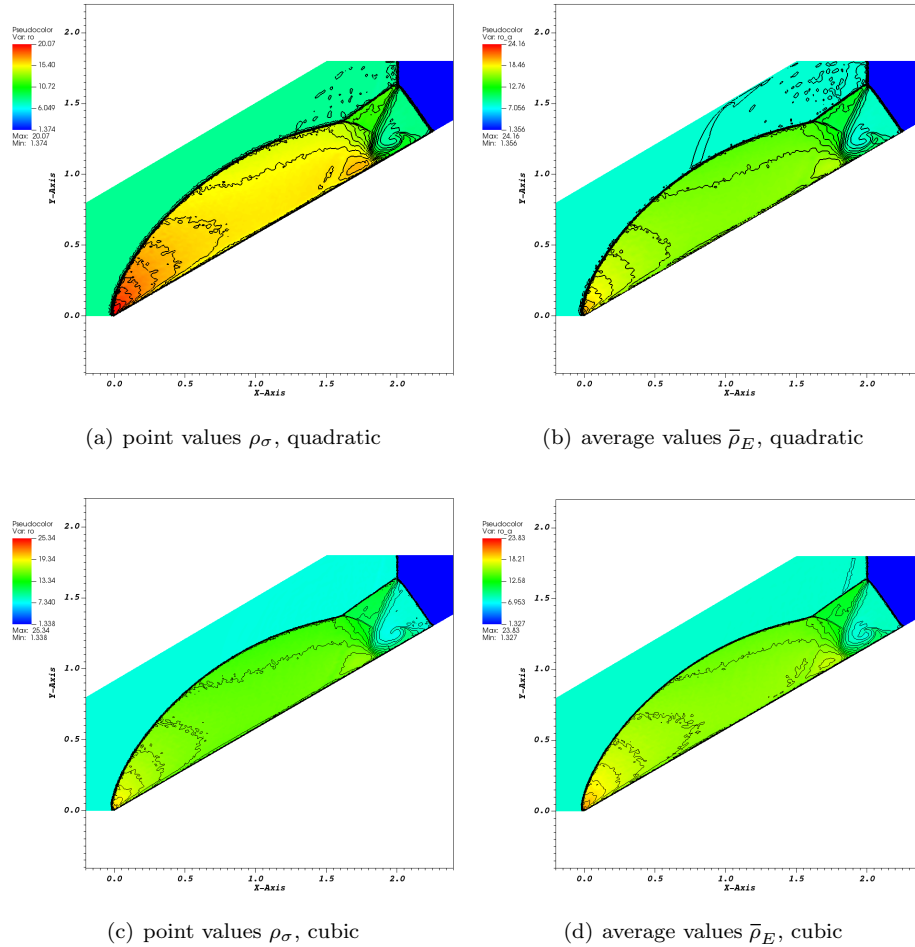


Figure 15: Woodward-Collela problem: profiles of density.

- [6] Remi Abgrall and Wasilij Barsukow. Extensions of active flux to arbitrary order of accuracy. ESAIM, Math. Model. Numer. Anal., 57(2):991–1027, 2023.
- [7] W. Barsukow. The active flux scheme for nonlinear problems. J. Sci. Comput., 86(1):Paper No. 3, 34, 2021.
- [8] S. Clain, S. Diot, and R. Loubère. A high-order finite volume method for systems of conservation laws—Multi-dimensional Optimal Order Detection (MOOD). J. Comput. Phys., 230(10):4028–4050, 2011.
- [9] H. Deconinck and M. Ricchiuto. Encyclopedia of Computational Mechanics, chapter Residual distribution schemes: foundation and analysis. John Wiley & sons, 2007. DOI: 10.1002/0470091355.ecm054.
- [10] T.A. Eyman. Active flux. PhD thesis, University of Michigan, 2013.
- [11] T.A. Eyman and P.L. Roe. Active flux. 49th AIAA Aerospace Science Meeting, 2011.
- [12] T.A. Eyman and P.L. Roe. Active flux for systems. 20 th AIAA Computational Fluid Dynamics Conference, 2011.

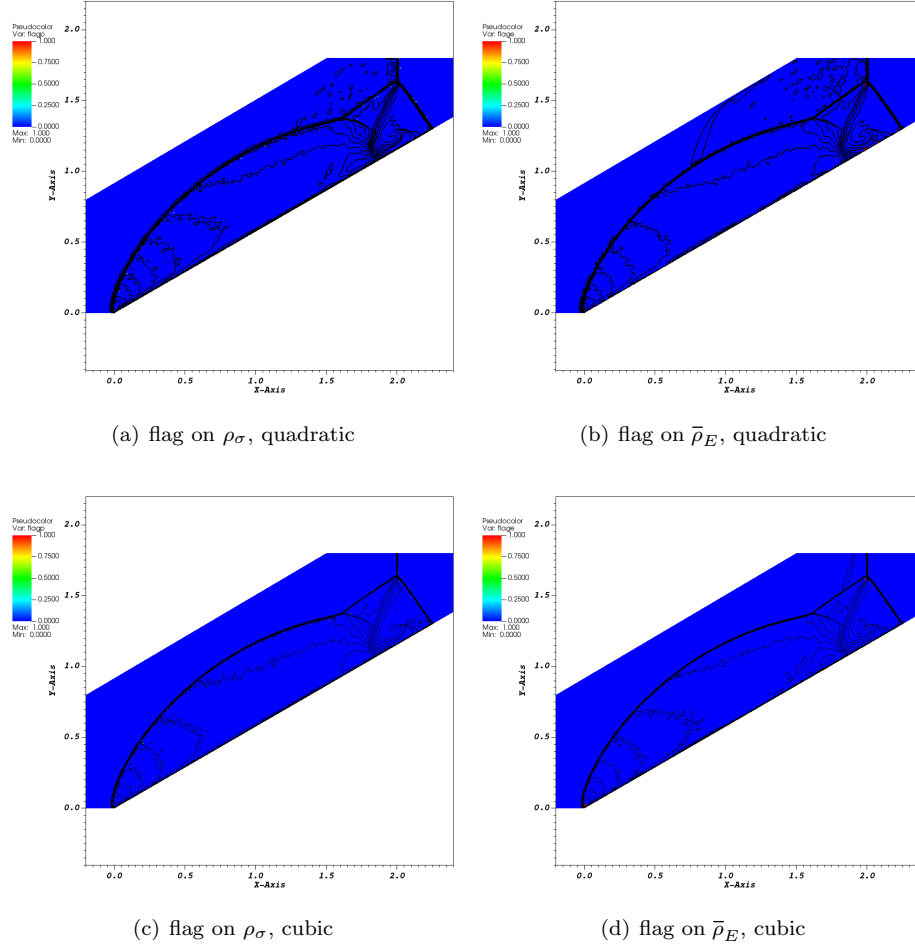


Figure 16: Woodward-Collela problem: flags at the positions where the first-order scheme is used.

- [13] E. Gaburro, W. Boscheri, S. Chiochetti, C. Klingenberg, V. Springel, and M. Dumbser. High order direct Arbitrary-Lagrangian-Eulerian schemes on moving Voronoi meshes with topology changes. *Journal of Computational Physics*, 407:109167, 2020.
- [14] Christophe Geuzaine and Jean-François Remacle. Gmsh: a 3-D finite element mesh generator with built-in pre- and post-processing facilities. *Int. J. Numer. Methods Eng.*, 79(11):1309–1331, 2009.
- [15] N. K. Grag, A. Kurganov, and Y. Liu. Semi-discrete central-upwind Rankine-Hugoniot schemes for hyperbolic systems of conservation laws. *Journal of Computational Physics*, 428:110078, 2021.
- [16] C. Helzel, D. Kerkmann, and L. Scandurra. A new ADER method inspired by the active flux method. *Journal of Scientific Computing*, 80(3):35–61, 2019.
- [17] A. Kurganov, Y. Liu, and V. Zeitlin. Numerical dissipation switch for two-dimensional central-upwind schemes. *ESAIM Mathematical Modelling and Numerical Analysis*, 55:713–734, 2021.
- [18] Alexander Kurganov, Guergana Petrova, and Bojan Popov. Adaptive semidiscrete central-upwind schemes for nonconvex hyperbolic conservation laws. *SIAM J. Sci. Comput.*, 29(6):2381–2401, 2007.

- [19] Alexander Kurganov and Eitan Tadmor. Solution of two-dimensional Riemann problems for gas dynamics without Riemann problem solvers. Numer. Methods Partial Differ. Equations, 18(5):584–608, 2002.
- [20] Xu-Dong Liu and Peter D. Lax. Solution of two-dimensional riemann problems of gas dynamics by positive schemes. SIAM J. Sci. Comput., 19:319–340, 1998.
- [21] John J. H. Miller. On the location of zeros of certain classes of polynomials with applications to numerical analysis. J. Inst. Math. Appl., 8:397–406, 1971.
- [22] E. van der Weide. Compressible Flow Simulations on Unstructured Grids using Multi-dimensional Upwind Schemes. PhD thesis, Delft University of Technology, 1998.
- [23] Bram van Leer. Upwind and high-resolution methods for compressible flow: From donor cell to residual-distribution schemes. Communications in Computational Physics, 1(2):192–206, 2006.
- [24] F. Vilar. *A posteriori* correction of high-order discontinuous Galerkin scheme through subcell finite volume formulation and flux reconstruction. J. Comput. Phys., 387:245–279, 2019.
- [25] B.-S. Wang, W. Don, A. Kurganov, and Y. Liu. Fifth-order A-WENO schemes based on the adaptive diffusion central-upwind Rankine-Hugoniot fluxes. Communications on Applied Mathematics and Computation, 5:295–314, 2023.
- [26] P. Woodward and P. Colella. The numerical solution of two-dimensional fluid flow with strong shocks. Journal of Computational Physics, 54:115–173, 1988.